Ultrasonics Sonochemistry 95 (2023) 106377

Contents lists available at ScienceDirect

Ultrasonics Sonochemistry

journal homepage: www.elsevier.com/locate/ultson

From crystal phase mixture to pure metal-organic frameworks – Tuning pore and structure properties

Przemysław J. Jodłowski [a,1,*], Grzegorz Kurowski [a], Klaudia Dymek [a], Marcin Oszajca [b], Witold Piskorz [b], Kornelia Hyjek [a], Anna Wach [c], Anna Pajdak [d], Michal Mazur [e,2], Daniel N. Rainer [e,3], Dominik Wierzbicki [c,f], Piotr Jeleń [g], Maciej Sitarz [g]

[a] Faculty of Chemical Engineering and Technology, Cracow University of Technology, Warszawska 24, 30-155 Kraków, Poland
[b] Faculty of Chemistry, Jagiellonian University, Gronostajowa 2, 30-387 Kraków, Poland
[c] Paul Scherrer Institute, 5232 Villigen, Switzerland
[d] Strata Mechanics Research Institute, Polish Academy of Sciences, Reymonta 27, 30-059 Kraków, Poland
[e] Department of Physical and Macromolecular Chemistry, Faculty of Science, Charles University, Hlavova 8, Prague 128 43, Czech Republic
[f] Faculty of Energy and Fuels, AGH University of Science and Technology, Mickiewicza 30, 30-059 Kraków, Poland
[g] Faculty of Materials Science and Ceramics, AGH University of Science and Technology, Mickiewicza 30, 30-059 Kraków, Poland

ARTICLE INFO

Keywords:
Metal–organic frameworks
Sonochemistry
Hf-MIL-140A
UiO-66

ABSTRACT

In this study, a sonochemical route for the preparation of a new Hf-MIL-140A metal–organic framework from a mixture of UiO-66/MIL-140A is presented. The sonochemical synthesis route not only allows the phase-pure MIL-140A structure to be obtained but also induces structural defects in the MIL-140A structure. The synergic effect between the sonochemical irradiation and the presence of a highly acidic environment results in the generation of slit-like defects in the crystal structure, which increases specific surface area and pore volume. The BET-specific surface area in the case of sonochemically derived Zr-MIL-140A reaches 653.3 m^2/g, which is 1.5 times higher than that obtained during conventional synthesis. The developed Hf-MIL-140A structure is isostructural to Zr-MIL-140A, which was confirmed by synchrotron X-ray powder diffraction (SR-XRD) and by continuous rotation electron diffraction (cRED) analysis. The obtained MOF materials have high thermal and chemical stability, which makes them promising candidates for applications such as gas adsorption, radioactive waste removal, catalysis, and drug delivery.

1. Introduction

Metal-organic frameworks (MOFs) have attracted the scientific community due to their widespread potential application in various fields including materials science, medicine, environmental protection, catalysis, and gas adsorption and separation. The idea of building novel structures composed of transition-metal carboxylate clusters connected with the organic linker is developing extremely intensively, as exemplified by the number of developed MOF structures exceeding 100,000.

Of the numerous reported MOF structures, those based on zirconium clusters are of particular interest to scientists due to their high thermal and chemical stability, large surface area, the presence of Lewis and Brønsted acidity, and the possibility of comprehensive synthesis and post-synthesis modification [1,2]. Since the first publication defining metal–organic frameworks by Yaghi and Li in 1995 [3], the discovery of zirconium-based metal–organic frameworks such as UiO-66, UiO-67, and UiO-68 [4], NU-1000 [5], DUT-67 [6] and PCN-224 [7] was another milestone in MOF development. More than 10 years after its discovery, UiO-66 has become the unwritten standard of zirconium-based MOFs due to its ease of synthesis, low price, and wide variety of applications [8]. The UiO-XX (X-designation of the next number of the described MOF form in UiO-family) may be summarized by the formula $Zr_6O_4(OH)_4(L)_6$, where L corresponds with terephthalate for UiO-66, 4,4′-biphenyldicarboxylate for UiO-67 and 4,4′-terphenyldicarboxylate

* Corresponding author.
E-mail address: przemyslaw.jodlowski@pk.edu.pl (P.J. Jodłowski).
[1] ORCID: 0000-0003-2554-6539.
[2] ORCID: 0000-0001-5044-5284.
[3] ORCID: 0000-0002-3272-3161.

https://doi.org/10.1016/j.ultsonch.2023.106377
Received 30 January 2023; Received in revised form 16 March 2023; Accepted 17 March 2023
Available online 21 March 2023

for UiO-68 [1]. The rapid development of MOF chemistry and its application has resulted in the development of numerous novel Zr-MOF structures. However, in some cases, instead of a single framework for a given metal–ligand combination, two or three MOF analogs were reported [9]. An example of such a related material for UiO-66 is Zr-MIL-140A, where the latter is composed of zirconium-based nodes connected with terephthalates giving rise to one-dimensional channels instead of three-dimensional ones observed between the clusters in UiO-66. The Zr-MIL-140A structure, which was first reported by Guillerm *et al.* [10], exhibits hydrophobic character, Lewis acidity, and high hydrothermal stability, which are highly demanded in catalysis. Over the years, numerous synthesis methods to obtain the MIL-140 family have been proposed, and their potential application in the field of adsorption [11,12], sensing [13], water desalination [14], and catalytic phenol hydrogenation [15]. The literature review exhibits two structures of MIL-140 built originally by $Zr_6O_4(OH)_4$ oxoclusters [10] and its Ce analog [16]. In work by Guillerm *et al.* [10], the MIL-140 family was denoted by suffixes from A-D, varying the organic linker used during the synthesis. The possible linkers include MIL-140A – 1,4-benzenedicarboxylic acid (BDC), MIL-140-B – naphthalene-2,6-dicarboxylic acid (NDC), MIL-140C – biphenyl-4,4′-dicarboxylic acid (4,4′-BPDC) and MIL-140D – 3,3′-dichloro-4,4′-azobenzenedicarboxylic acid (Cl_2-AzoBDC). In that work, the molar ligand-to-metal ratio was kept 2:1, with the DMF amounts of equal 125 mL, 15 mL, 25 mL, and 5 mL for MIL-140A, MIL-140B, MIL-140C, and MIL-140D, respectively. The synthesis temperature was equal to 220 °C for MIL-140A-C structures, whereas for MIL-140D was equal to 180 °C. The resulting MIL-140A and MIL-140C crystallized in the *C*2/*c* space group, whereas the space group changes to Cc for MIL-140B and MIL-140D, respectively. It is worth mentioning that the S_{BET} and pore volume of MIL-140A-D increase with an increasing length of the linker.

In the literature, the cerium-based MOFs from the UiO family were first reported by Lammert *et al.* [16]. In their work, they reported Ce-UiO-66 structure which is isoreticular to Zr-UiO-66. In work by Jacobsen *et al.* [17], the solvothermal synthesis of Ce-MIL-140A used terephthalic acid (H_2BDC), 2-chloroterephthalic acid (H_2BDC-Cl), and 2,6-naphtalenedicarboxylic acid (H_2NDC) as organic linkers. The detailed parameters of reported Ce-MIL-140A are summarized in Table 1. It is worth mentioning that the resulting crystal structure of Ce-MIL-140A differs from its Zr-MIL-140A analog reported elsewhere [10]. The Ce-MIL-140A crystallizes in the triclinic symmetry in comparison to the monoclinic in the case of Zr-MOF-140A. As reported by Jacobsen *et al.* [17], a decrease in specific surface area may be also observed. The decrease of S_{BET} to 222 m^2/g in the case of Ce-MIL-140A is supposed to be due to the pore blockage of residual DMF after the activation process.

Apart from high-temperature synthesis [16,17], in work by Schulz *et al.* [18], the low-temperature synthesis of MIL-140A frameworks at 120 °C and 150 °C was reported. The work focuses on the influence of synthesis conditions such as DMF concentration, metal-to-linker ratio, and the addition of an acetic acid modulator on the phase purity of MIL-140A samples.

Over the years, numerous methods of MOF synthesis have been developed using several methods, the most used are solvothermal, mechanochemical, microwave, and sonochemical methods. Although solvothermal, mechanochemical, and microwave methods are the most utilized in the literature, the sonochemical synthesis of metal–organic frameworks seems to be still not fully explored area.

Sonochemistry is a branch of science on the border of physics and chemistry, dealing with the impact of ultrasonic waves on their surroundings. Sonochemistry is also called “green synthesis”, due to the considerable or even maximal reduction of harmful solvents involved during both inorganic and organic synthesis. The chemical effects of ultrasound irradiation are not caused by the interaction of acoustic waves on the atomic and microscopic levels, but are induced by acoustic cavitation which is an effect of ultrasonic irradiation on the liquid system [19-21]. Since the first work on the use of sonication appeared in 2008, reporting the synthesis of $[Zn_3(BTC)_2]$ [22], only a few more known MOF structures have been reported so far. The initial goal of the use of sonochemical irradiation for the preparation of MOF structure was to find rapid, low energy consuming, and repeatable synthesis of MOFs that would allow their facile industrial synthesis.

An exemplary work describing the synthesis of metal–organic frameworks by using ultrasound irradiation was presented by Son *et al.* [23]. The authors used a 200 W ultrasound horn to synthesize MOF-5. The preparation of MOF material was performed over various times (10–75 min) and sonication powers (10–50% of maximum power). As a reference, conventional heat-treatment synthesis of MOF-5 was performed, with the maximum crystallization time of 24 h. As a result, the sonochemical preparation method revealed that the crystallization of MOF-5 started just after sonication began, whereas in conventional methods white MOF-5 crystals began to precipitate after 12 h. In other work [24], the preparation of MIL-88A using ultrasound irradiation was reported where an ultrasound bath was used instead of an ultrasound horn. The authors reported the synthesis of MOF crystals at temperatures 0–50 °C and times 0–10 min. The synthesis of MIL-88A was performed using the microwave route. Both methods allowed for the synthesis of MIL-88A, but any comparison between them is impossible. The maximum temperature in the ultrasound preparation method was

Table 1
Sample details.

Sample	Formula	Refinement	Crystal system	Space group	A, (Å)	α,(°)	S_{BET}, (m^2/g)	S_L, (m^2/g)	V_{DFT}, (cm^3/g)
Hf-MIL-140A	$Hf_8O_{40}C_{64}H_{32}$	Rietveld	Monoclinic	*C*2/*c*	a = 25.5983(7) b = 11.1775(3) c = 7.8086(2)	α = 90.000 β = 112.591 (2) γ = 90.000	425.1	846.2	0.305
Zr-MIL-140A	$Zr_8O_{40}C_{64}H_{32}$	Rietveld	Monoclinic	*C*2/*c*	a = 25.6368(16) b = 11.2048(7) c = 7.8254(4)	α = 90.000 β = 112.417 (6) γ = 90.000	653.3	956.0	0.338
Zr-MIL-140A [10]	$Zr_8O_{40}C_{64}H_{32}$	Rietveld	Monoclinic	*C*2/*c*	a = 24.424(1) b = 11.1795(1) c = 7.802(1)	α = 90.000 β = 103.861 (2) γ = 90.000	415(10)	–	0.176
Ce-MIL-140A [17]	$Ce_8C_{64}O_{40}H_{32}$	Rietveld	Triclinic	$P\bar{1}$	a = 8.1690(3) b = 11.5516(3) c = 13.9869 (5)	α = 113.099 (3) β = 102.331 (4) γ = 90.488(5)	222	–	0.103

S_{BET} is the specific surface area according to BET model; S_L is the specific surface area according to Langmuir model; V_{DFT} is total pore volume according to DFT model; detailed low temperature N_2 analysis and S_{BET} fitting can be found in Supporting Information File.

maintained at 50 °C, whereas the temperatures in the microwave route were as high as 120 °C. Similar trends can be also observed for reaction times.

In the work by Sabouni *et al.* [25], the preparation of IRMOF-1 by combined sonochemical-microwave methods is presented. As a result, the authors obtained well-crystallized IRMOF-1 powders with specific surface areas varying from 1300-2400 m^2/g.

Indeed, the above-mentioned literature data provide information about high yields, shorter reaction times, and even room temperature synthesis of MOF structures using sonochemical methods. However, the questions arise: I) whether ultrasound irradiation may be successfully used as a driving force to build the structure of the pure MOF from the mixture of MOFs, and II) how the sonication changes the overall MOF structure.

In this work, the sonochemical synthesis route of Zr-MIL-140A and, for the first time, Hf-MIL-140A from the mixture of UiO-66 and MIL-140A metal–organic frameworks is described. It was shown, that the sonochemical irradiation of mixture UiO-66 and MIL-140A in a mixture of acetic acid and methanol results not only in the formation of pure phase MIL-140A structure but generates slit-shape micropores increasing the BET specific area by about 50% compared to MIL-140A obtained from conventional solvothermal synthesis.

2. Experimental

The detailed information about the chemicals used in this study is summarized in Table S1 in the Supporting Information File.

The sonochemical synthesis of Me-MIL-140A (Me – Zr or Hf) metal–organic frameworks was performed in a two-step approach. In the first step, the Me-MIL-140A precursor (Pre-MIL-140A (Me – Zr or Hf)) was synthesized using the solvothermal method described elsewhere [18], with some modifications. The synthesis parameters were adjusted to obtain a mixture of UiO-66 and MIL-140A which was the precursor for further sonochemical treatment. The detailed synthesis parameters of Pre-MIL-140A (Me – Zr or Hf) are summarized in Table S2.

In the next step, the as-prepared Pre-MIL-140A (Me – Zr or Hf) was further sonicated by using the QSonica Q700 sonicator equipped with a ½" diameter horn. Typically, 200 mg of Pre-MIL-140A (Me – Zr or Hf) was suspended in a mixture of methanol and appropriate acid solution (see Table S3). The resulting suspension was placed in an ice bath. Then, the suspension was treated by using the appropriate sonication parameters including sonication time and amplitude. Prior to the sonication, the suspension was purged with 50 mL/min Ar flow for 10 min. The detailed sonication conditions are summarized in Table S3. The resulting crystals were centrifuged and washed three times with methanol, dried at room temperature, and then activated in a vacuum drier at 120 °C for 10 h. During the sonochemical syntheses, the ultrasonic horn was placed in a 100 mL round bottom flask with a fixed distance between the tip-flask bottom equal to 12 mm.

Hf-MIL-140A was also synthesized via the solvothermal method by dissolving the 2 mmol (653 mg) of $HfCl_4$ and 4 mmol (664 mg) of terephthalic acid in a mixture of 6 mL glacial acetic acid and 6 mL DMF. The resulting solution was then transferred to Teflon liners. The prepared stainless-steel autoclaves with Teflon lining were placed in an oven at 220 °C for 20 h. The resulting crystals were filtered from the solution. The white crystals were washed three times in DMF and then washed three times with methanol. The resulting materials were then dried at room temperature and then activated in a vacuum drier at 120 °C for 10 h. The synthesis details are summarized in Table S4.

The obtained MOF samples were characterized by using various techniques including SR-PXRD, cRED, XAS/EXAFS, μRaman, *in situ* FTIR, SEM, STEM, low-temperature N_2 adsorption, and elemental analysis. The characterization details are described in the Supporting Information File.

3. Results and discussion

3.1. Solvothermal synthesis of Pre-MIL-140A (Me – Zr or Hf)

The influence of solvothermal synthesis parameters on purity of MIL-140A crystals was described in detail in work by Schulz *et al.* [18]. The analysis of the phase diagram presented in their work indicates two areas in which appropriate crystals are formed. They found that at the concentrations above 80 equivalents of DMF used during the synthesis, both crystalline phases of UiO-66 and MIL-140A were present in the reaction mixture. The increase of the DMF concentration, while keeping the linker to $ZrCl_4$ constant, results in the formation of a pure UiO-66 structure. The formation of the MIL-140A structure proceeds at concentrations below 60 equivalents. The formation of the MIL-140A structure is the result of incomplete linker dissolution or a strongly acidic reaction. Additionally, Schulz *et al.* [18] found that at DMF concentrations of up to 60 equivalents and upon the addition of acetic acid of up to 30 equivalents, pure MIL-140A is formed. Only for synthesis mixtures containing 20 equivalents of DMF and 30 equivalents of acetic acid the "preliminary phase" consisting of the mixture of UiO-66 and MIL-140A was obtained, which crystallizes to MIL-140A upon increasing the reaction time to 72 h. The second region in UiO-66/MIL-140A system indicates that at DMF concentrations in a range of 80–100 equivalents and acetic acid in a range of 10–30 equivalents the mixture of UiO-66/MIL-140A is obtained. It is worth mentioning that originally in the work of Guillerm *et al.* [10], the synthesis of MIL-140A MOF was performed at 220 °C for 16 h using a 2:1 linker-to-$ZrCl_4$ ratio and without the addition of any of the modulators. The results of the work of Schulz *et. al.* [18] cannot be simply applied to our system, since in our experiments the original linker to $ZrCl_4$ ratio was preserved and the temperature was kept at 220 °C for 20 h (Table S2). Additionally, in the synthesis of the Pre-MIL-140A (Me – Zr or Hf) system, a small amount of hydrochloric acid was used to promote the formation of UiO-66 in the overall mixture. According to our results, the mixture of UiO-66/MIL-140A was obtained not only for the zirconium counterpart but also when using $HfCl_4$ as a metal source. Additionally, the $–NH_2$ analogs were successfully obtained when using 2-aminoterephthalic acid instead of terephthalic acid. Furthermore, when using the 2-hydroxyterephthalic acid to obtain –OH analogue in the Pre-MIL-140A (Me – Zr or Hf) the synthesis did not result in the formation of any of the crystals.

The successful preparation of Hf-MIL-140A and Zr-MIL-140A was performed by sonochemical irradiation applied to the mixture of UiO-66 and MIL-140A (Pre-MIL-140A (Me – Zr or Hf)) obtained by solvothermal method. It should be pointed out that the sonochemical synthesis of both Hf and Zr-MIL-140A from Pre-MIL-140A (Me – Zr or Hf) was possible only when the mixture of UiO-66 and MIL-140A was obtained during the solvothermal synthesis and appropriate sonochemical irradiation parameters (*cf.* Table S2 and Table S3). The direct sonication of the MOF precursors, however, did not result in the formation of either UiO-66 or MIL-140A structures. The foregoing solvothermal synthesis of Pre-MIL-140A followed by sonochemical irradiation was necessary to obtain pure Hf or Zr-MIL-140A structures.

3.2. Crystal structure of Hf-MIL-140A

The crystal structures of both Hf-MIL-140A and Zr-MIL-140A were determined based on the data collected from the SR-PXRD experiments and refined by applying the Rietveld method (Table S5). The representation of the crystal structure of Hf-MIL-140A is shown in Fig. 1. The new MOF presented in this study can be characterized by the formula $Hf_8H_{32}C_{64}O_{40}$ which is related to the Hf-UiO-66 structure [26]. The chains present in the model propagate along [001] direction with the repeat period of *c/2*. The shared edges contain the only crystallographically independent oxygen atom of the structure that is not a part of the terephthalic acid molecule, an oxo-μ3 atom. The rest of the O-vertices of the capped octahedra correspond to one of the oxygen atoms

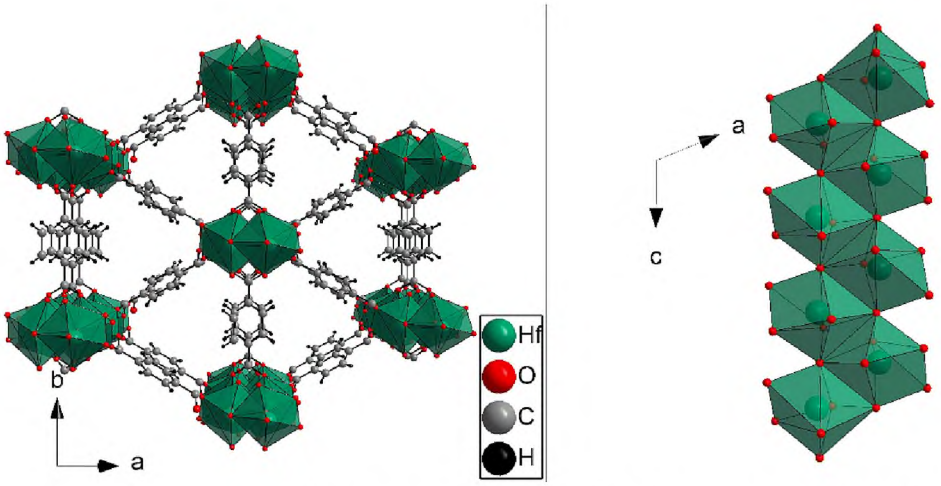

Fig. 1. Crystal structure of Hf-MIL-140A; (B) Inorganic building unit of Hf-MIL-140A; Hf - green, O - red, C - graphite, H - black.

from two structurally independent terephthalic acid molecules lying in special positions. The molecules interconnect "the inorganic fibers" along [0 1 0] direction (molecule positioned along the twofold axis with coordinates 0, y, ¼ and all symmetrically related – Wyckoff site e) and along two symmetrically related directions almost ideally parallel to [1 1 1] and [1-11] (the geometric center of the molecule is positioned on an inversion center at coordinates ¼, ¾, ½, and all symmetry-related ones – Wyckoff site c). Fig. 1A presents the projection of the structure along the fiber propagation direction displaying the arrangement of the organic molecules connecting the fibers. This projection also highlights the channels formed between the fibers and organic molecules. The channels present in the structure are interconnected into two separate groups (*x*-coordinate in the 0–0.5 range and 0.5–1 range) which are responsible for the sorption properties of the studied material. Fig. 1B highlights the arrangement of the Hf polyhedra that allows the formation of the fibers. The accompanying structure of Zr-MIL-140A is presented in Figure S1.

Initially, the model of the structure was solved in the *Cc* space group and contained a fiber formed by edge-sharing capped octahedra composed of Zr centers and O vertices. But, as the DFT calculations performed on the Rietveld refined (Fig. 2) model revealed the introduction of an inversion center does not affect the stability of the calculations or impact the results in a meaningful way. Additionally, considering the published structure of MIL-140A, the final solution was pursued in *C 2/c* space group. The Rietveld refinement yielded a satisfactory fit of the refined model to the registered data, see Fig. 2.

3.3. *Purification of mixture of UiO-66/MIL-140A by sonochemical irradiation to obtain (Me – Zr or Hf)-MIL-140A*

Based on our previous experience with the use of ultrasonic irradiation to obtain crystalline materials, the high-gain ultrasound treatment on Pre-MIL-140A (Me – Zr or Hf) crystals and, in the next step, rebuilding of the crystal structure to obtain pure (Me – Zr or Hf)-MIL-140A from a mixture of UiO-66/MIL-140A was deemed necessary. Initially, the high gain ultrasounds were expected to generate mesoporosity in the UiO-66/MIL-140A structure or, due to the presence of highly acidic conditions and the presence of free radicals that are formed during the sonolysis [27], the mixture of UiO-66/MIL-140A would decompose and the MOF structure would be damaged. In the work by Chu *et al.* [28], the mechanism of dilution/regeneration of UiO-66 in acidic media was examined. In their work, UiO-66 was placed in the ammonium bicarbonate aqueous solution which caused the dilution of the pristine UiO-66 structure yielding a colorless, clear solution. In the next step, acetic acid, DMF, and benzoic acid were added to the mixture. The resulting mixture was transferred to the autoclave and then heated at 150 °C for 48 h. In the sonochemical method presented in our study, the Pre-MIL-140A (Me – Zr or Hf) structure is treated in a highly acidic acetic acid and methanol mixture which is then treated with high-gain ultrasounds. Although, by comparing the acidity of the reactants used in our study with those found in work by Chu *et al.* [28], it can be concluded that the mixture would eventually be expected to be diluted. However, the complete dissolution of obtained Pre-MIL-140A (Me – Zr or Hf) crystals was observed only in the case of Pre-MIL-140A-NH_2 (Me – Zr or Hf), whereas in other cases the crystals introduced into the sonication mixture remained present after the sonication process. When analyzing the resultant crystals, a correlation between the type of acid used during the sonochemical synthesis, sonication time, amplitude, and the purity of received crystals was found. The pure phase MIL-140A structure was obtained only in a presence of acetic acid using both acid/methanol ratios equal to 1:3 and 1:1 (Table S3, synthesis no. 4 and 7). On the contrary, in the sonochemical syntheses which were carried out in a mixture of acetic acid and hydrochloric acid using both acid/methanol ratios, the UiO-66 (Zr) structure was obtained (Table S3, synthesis no. 1 and 2). Similar observations were made when the synthesis was followed only in a methanol solution (Table S3, synthesis no. 3). Following this way of thought, the syntheses were conducted only in an acetic acid/methanol mixture. Evaluating the influence of sonication amplitude on crystal purity, it was found that the pure MIL-140A phase was obtained only at amplitudes equal to 60% even using a sonication time as short as 15 min. An increase in sonication time does not influence the phase composition. The same observations were made for Hf-MIL-140A.

3.4. *Characterization*

Low-temperature N_2 adsorption measurements of Hf-MIL-140A and Zr-MIL-140A structures (Fig. 3, Figure S2) resulted in type I adsorption isotherms characteristic of microporous materials (Fig. 3A). The main adsorption increase in the isotherms was in the p/p^0 range of $0–10^{-5}$ and the total sorption capacity at 0.1 MPa was at 316 cm^3/g STP (Zr-MIL-140A) and 252 cm^3/g STP (Hf-MIL-140A) confirming a presence of the diverse pores. The pore size distribution, determined according to the DFT model, distinguished pores with diameters in the range of 0.7–0.9 nm and 1.3–1.8 nm (Fig. 3B). In Hf-MIL-140A, the pore volume in the 0.7–0.9 nm range was lower than in Zr-MIL-140A and, in addition, mesopores in the range between 3 nm and 4 nm were opened. It must be pointed out that both specific surface area and total pore volume are considerably higher in case of Zr-MIL-140A. The specific surface area determined by using the BET model reported in the literature data for Zr-

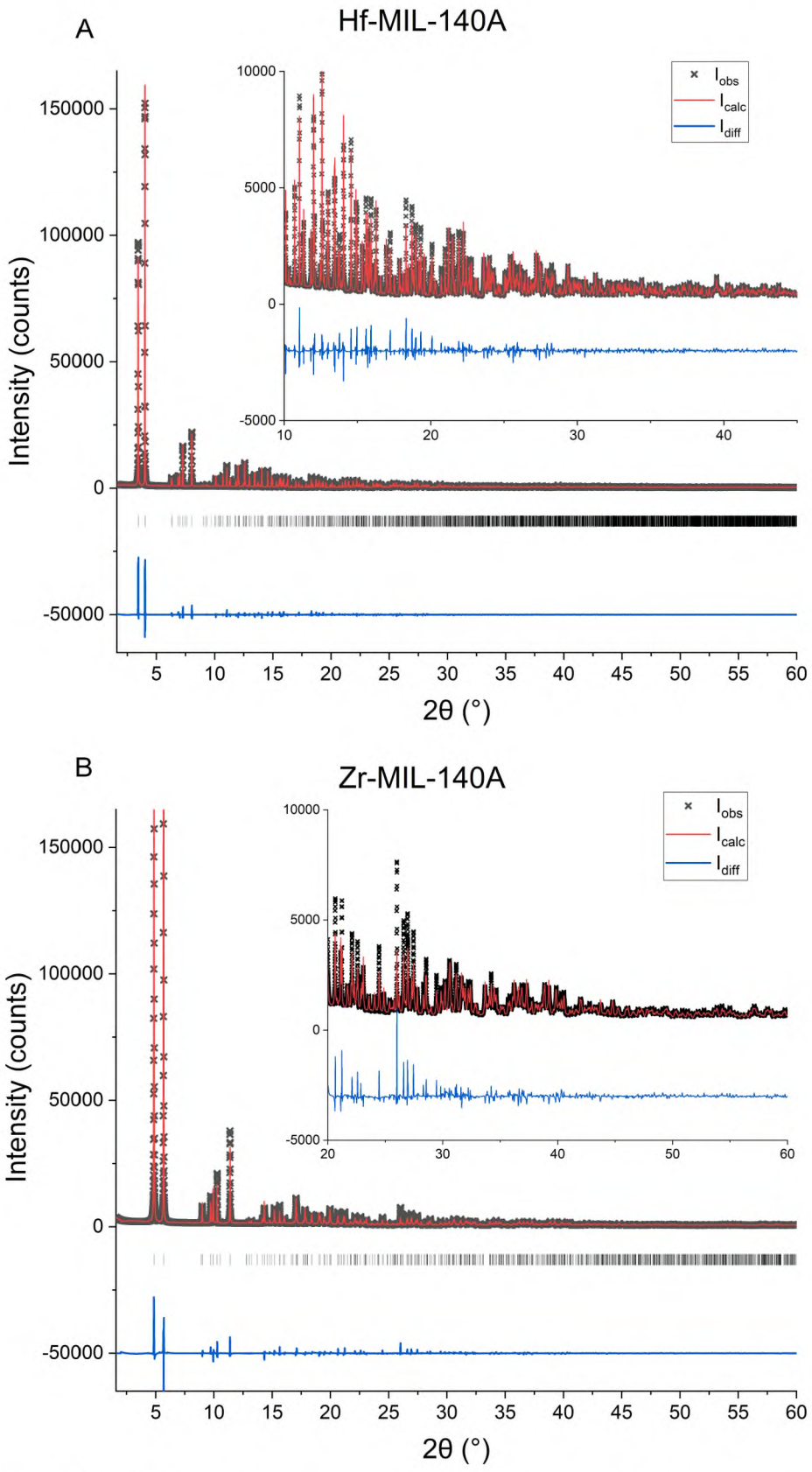

Fig. 2. Rietveld plots for **(A)** Hf-MIL-140A and **(B)** Zr-MIL-140A; SR-PXRD wavelength used: $\lambda_{HF\text{-}MIL\text{-}140A} = 0.70805$ Å, $\lambda_{Zr\text{-}MIL\text{-}140A} = 1.00410$ Å; insets - enhancement of the lower intensity regions.

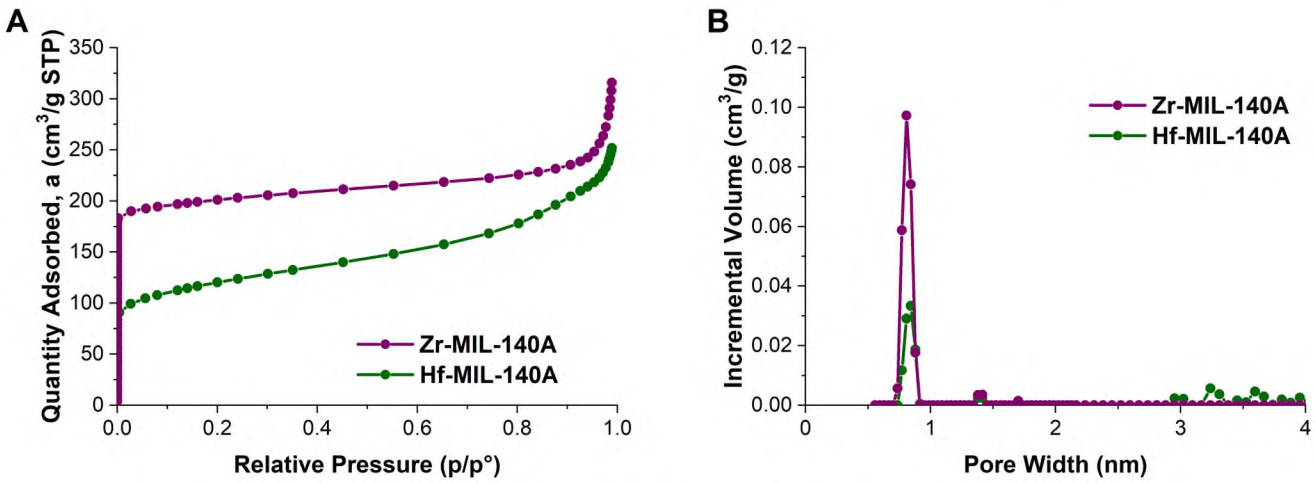

Fig. 3. (A) N_2 adsorption isotherms and (B) DFT pore size distribution of MIL-140A samples.

MIL-140A varies from 415 m^2/g [10], through 396 m^2/g [12] to 280 m^2/g [18]. In our work (Table 1, Figure S2), a 1.5-fold higher S_{BET} values (653 m^2/g) for the Zr-MIL-140A sample obtained in the sonochemical route was observed. Such a considerable increase is related to the presence of larger pores (DFT pore size distribution, Fig. 3B). It should be noted that the presence of these pores is related to the specific conditions used during the synthesis step. Under highly acidic conditions in the presence of high-gain ultrasounds, the MOF structure may be defected due to linker or node removal or both linker and nodes at the same time. In Hf-MIL-140A, a lower value of S_{BET} and V_{DFT} parameters was obtained than in Zr-MIL-140A and were equal to 425 m^2/g and 0.305 cm^3/g, respectively. Since the organic acid used will rather have a tendency to remove linkers, the latter mechanism cannot be rejected due to the possibility of simultaneous removal of linkers and nodes as previously reported for defective UiO-66 in work by Liu *et al.* [12]. The defect generation through the addition of organic and inorganic acids is commonly used for UiO-66 samples [29-34]. This mechanism, however, has not previously been sufficiently examined for MIL-140 MOFs. In the work by Schulz *et al.* [18], the Zr-MIL-140A samples were prepared with addition of 32 mmol acetic acid which resulted in a decrease of S_{BET} from 415 m^2/g reported in [10] to 280 m^2/g [18]. By comparing the results of S_{BET} by using the modulator during the MOF synthesis in the MIL-140 family with UiO-66, a reversed tendency can be observed. In the work by Shearer *et al.* [34], the influence of a modulator on S_{BET} increase was shown and the correlation between an increase of S_{BET} with an increasing concentration of acid used during the synthesis was observed. Since in the MIL-140A system this tendency was reversed, it cannot be firmly stated that in the case of using a high concentration of acid during the synthesis without the influence of ultrasound, it has no effect on the size of the BET surface. Due to the fact that the effect of ultrasound on the synthesis of MOF is insufficiently investigated, further research on the sonochemical synthesis and on the correlation of ultrasound power-modulator concentration is needed.

The morphology of prepared samples was determined by SEM/EDS and STEM analyses (Fig. 4 and Fig. 5). Based on SEM images of Hf-MIL-140A, it is characterized by a flake-like crystal habit with an average size of around 1 μm (Fig. 4A-C). The analysis of the SEM images at higher magnifications shows that the crystals exhibit a terrace-like structure with an average plate thickness of *ca.* 100 nm. The Hf-MIL-140A morphology does not differ from its Zr-MIL-140A analog (Figure S3), and is in good agreement with the results reported in the literature for Zr-MIL-140A synthesized by conventional methods [18]. The SEM/EDS maps of both Hf-MIL-140A and Zr-MIL-140A (Figure S4 and Figure S5) samples show a uniform distribution of elements throughout the entire particles.

Representative STEM images of the Hf-MIL-140A sample are shown in Fig. 5 and Figure S6 and for Zr-MIL-140A in Figure S7. As shown by SEM/EDS analysis, the crystals' flake-like structure was also confirmed by STEM analysis (Fig. 5A-B). At higher magnifications, the samples of Hf-MIL-140A show slit-like defects (width of *ca.* 1 nm) which are spread over the entire MOF crystal (Fig. 5C). Apart from slit-like defects, the presence of 5 nm holes was detected (Fig. 5D). The STEM images of both Hf-MIL-140A and Zr-MIL-140A samples are in good agreement with the structural models along [1 1 0] direction. Interestingly, the Hf-MIL-140A and Zr-MIL-140A images allow us to observe Hf and Zr nodes and the BDC ligands at the atomic level (Figures S6-S7 B and C).

To identify whether the structural defects are present in prepared samples, the comparative STEM images were performed (Figure S8 and Figure S9). The slit-like structural defects are clearly visible in both Hf-MIL-140A and Zr-MIL-140A. It must be pointed out, however, that the comparison of defects between Hf-MIL-140A and Zr-MIL-140A indicates that in the case of the Hf-MIL-140A sample the slits are wider, reaching *ca.* 5 nm. The high-resolution images (Figure S8 and Figure S9) show that the defects are arranged perpendicularly to the crystal lattices of

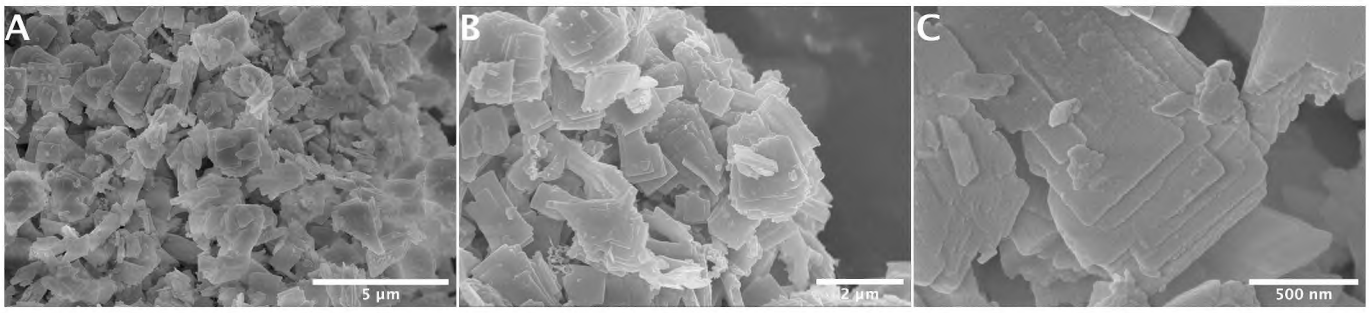

Fig. 4. SEM images of Hf-MIL-140A, (A) × 25 k, (B) × 40 k, (C) × 200 k.

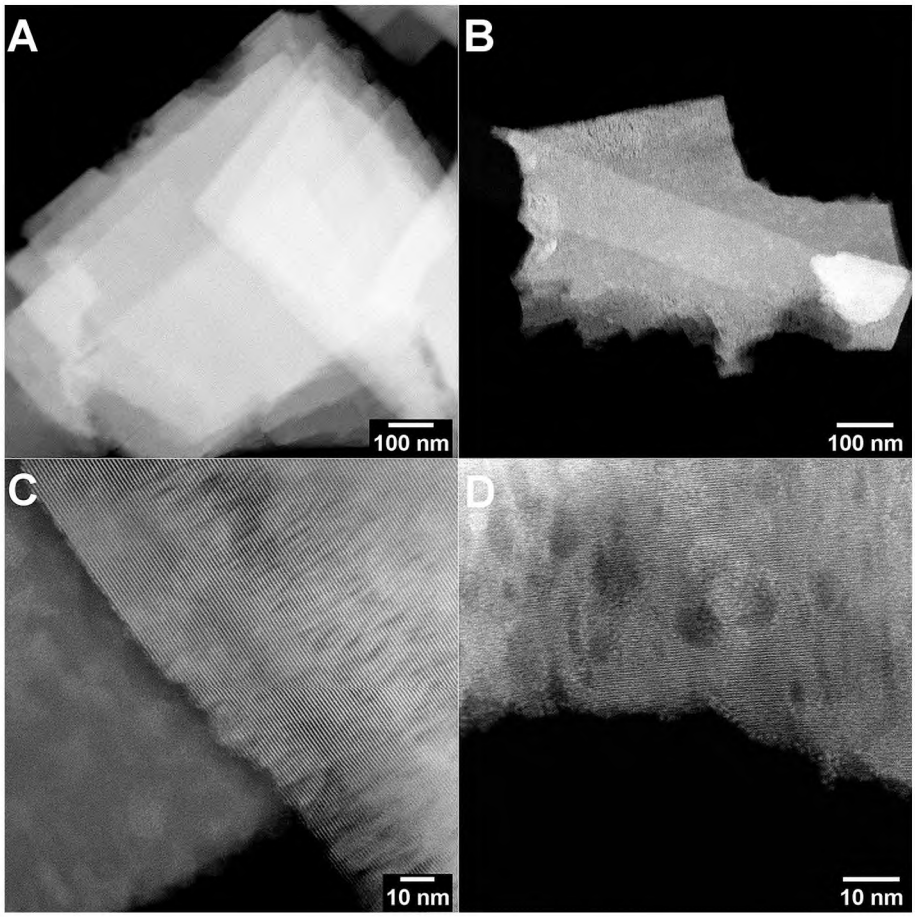

Fig. 5. STEM images of Hf-MIL-140A sample.

prepared MOFs. Moreover, the high-resolution images indicate that the crystal edges of Zr-MIL-140A remain even (Figure S9A), whereas the Hf-MIL-140A exhibits rugged edges (Fig. S8A).

In addition to the previously performed PXRD studies, the structures of prepared Hf- and Zr-MIL-140A materials were also determined by single crystal electron diffraction, using continuous rotation electron diffraction (cRED) (Table S6). The crystals were stable enough to be measured at room temperature without the need for cooling. Experiments and data processing were performed following Yang *et al.* [35], using the software Instamatic [36] for data collection, XDS [37] for data processing, and SHELXT [38] and SHELXL [39] for structure solution and refinement. Figures S10 and S11 show reciprocal lattice slices for Hf- and Zr- variants, respectively. The unit cell parameters as well as the final structures agree well with those obtained by SR-PXRD (*cf.* Table S5 and Table S6) and confirm the above-described structure models, comprising two symmetrically independent organic linker

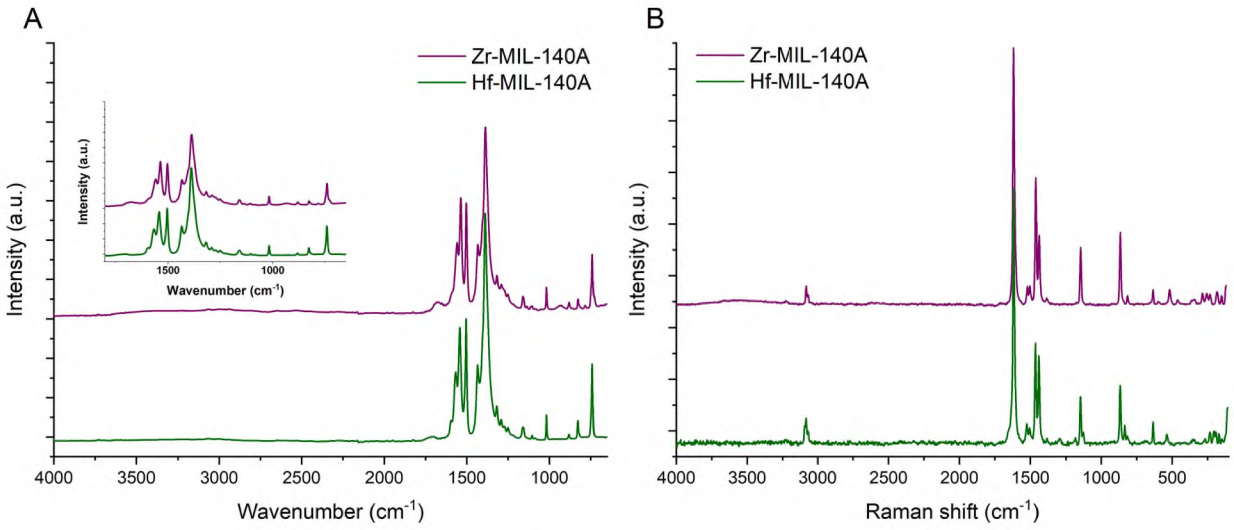

Fig. 6. (**A**) FTIR and (**B**) μRaman spectra of MIL-140A samples.

molecules connecting chains of metal oxide clusters to form the three-dimensional framework of MIL-140A.

The molecular nature of prepared samples was determined by FTIR and μRaman spectroscopies. The results are shown in Fig. 6 and Table S7. The FTIR spectra of the Hf-MIL-140A sample (Fig. 6A) show similar bands as the Zr-MIL-140A sample and are in good agreement with those found in the literature [17,40]. The Hf-MIL-140A reveals characteristic bands at 1560, 1536, and 1504 cm^{-1} which can be assigned to asymmetric COO^- stretching [41], respectively. The bands at 1387 cm^{-1} correspond with symmetric COO^- stretching vibrations [17]. The bands at 1159 and 1017 cm^{-1} may be assigned to in-plane C-H bending vibrations in terephthalates, whereas the bands at 826 and 740 cm^{-1} originate from aromatic out-of-plane C-H bending vibrations [17]. The μRaman spectra of the prepared samples are shown in Fig. 6B. The sharp band at 1620 cm^{-1} originates from C = C stretching vibrations [42] whereas the bands at 1462 and 1440 cm^{-1} originate from COO^- carboxylate vibrations [42]. The band at 1147 cm^{-1} may be assigned to aromatic ring deformation vibration, whereas the band at 868 cm^{-1} originates from C-H aromatic out-of-plane deformation vibration [41]. The weak band at the μRaman spectrum at 517 cm^{-1} may be attributed to Zr-O modes.

To investigate the thermal stability of sonochemically prepared Hf-MIL-140A, variable temperature *in situ* PXRD was performed (Fig. 7A). As can be noticed, the crystalline structure of the Hf-MIL-140A sample remains stable up to 450 °C which is 50 °C higher than for the Zr counterpart (*cf.* Figure S12). However, it must be emphasized that the thermal stability of MOFs is not only affected by the metal used for the MOF design, but also by the synthesis conditions such as temperature and solvent used during the synthesis [43]. As previously reported by Shearer *et al.* [43], the thermal stability of Zr-UiO-66 increases with an increasing synthesis temperature. Since in our study both the Hf- and Zr-MIL-140A samples were synthesized using the same conditions, the

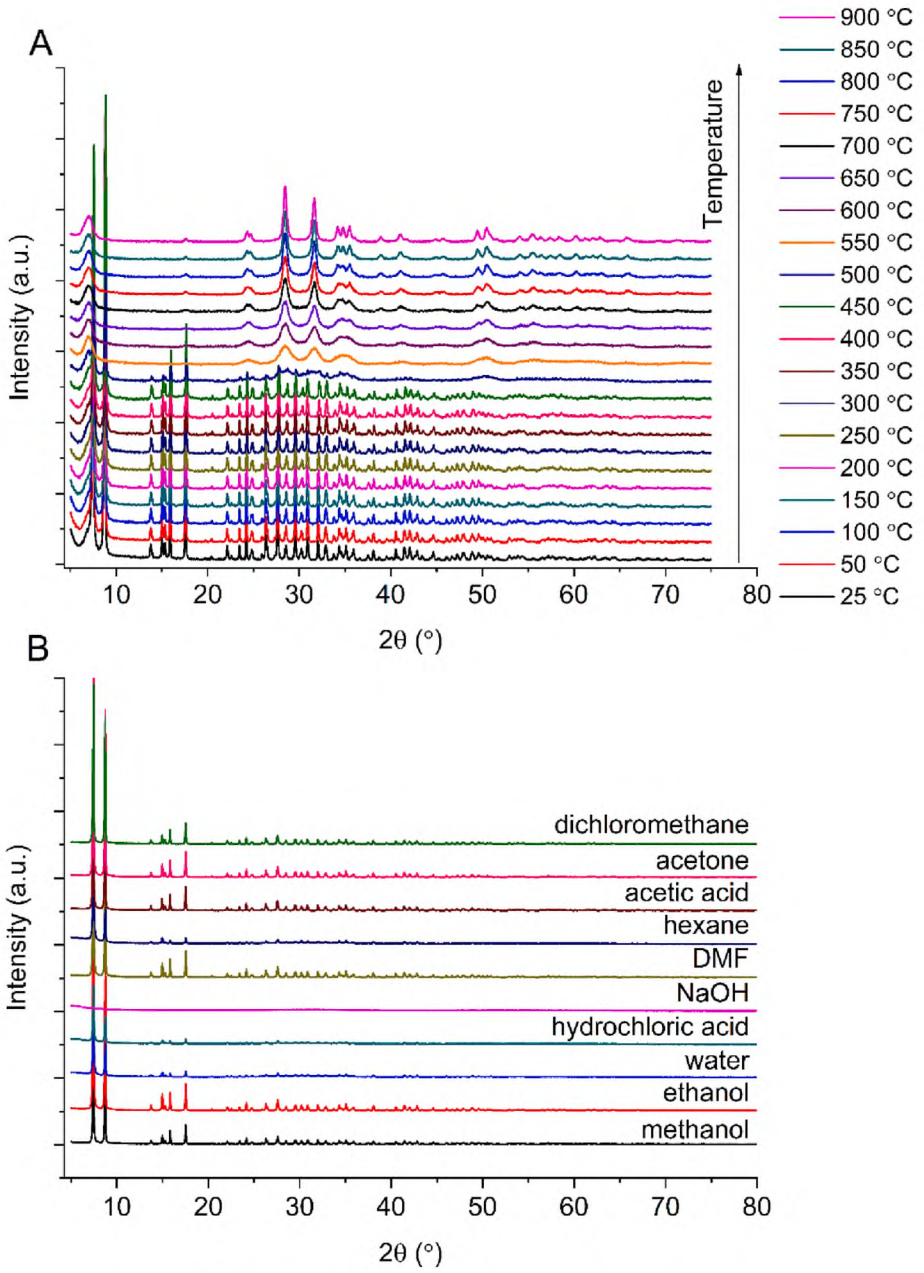

Fig. 7. (**A**) *In situ* high temperature PXRD results for Hf-MIL-140A synthesized by sonochemical route, (**B**) PXRD diffraction patterns for 24-hour stability test in different media for Hf-MIL-140A.

slightly higher thermal stability of Hf-MIL-140A should be rather limited to small differences in the degree of defect between samples. Since the research on MIL-140A defects exceeds the scope of this article, this issue will be the subject of our next research on the structure of Hf-MIL-140A.

The chemical stability of Hf-MIL-140A was checked in different media in 24 h stability tests. The PXRD diffractograms are shown in Fig. 7B. The results clearly show that the Hf-MIL-140A remains crystalline in a vast majority of media used during the experiments. The structure of Hf-MIL-140 collapses after treatment with NaOH solution. The decrease in crystallinity was observed in samples treated with hydrochloric acid and water. In comparison, the Zr-MIL-140A sample was also stable in most of the media used (Figure S13). However, it was observed that the sample becomes amorphous after treating by NaOH solution, and loss of crystallinity was observed after contact with hydrochloric acid. Additionally, a slight loss of crystallinity was observed after treating with dichloromethane. The determined superior thermal and chemical stability of the Hf-MIL-140A sample allows us to classify it in a series of MOFs with high chemical and thermal resistance on a par with UiO-66 or NU-1000 which opens up many application possibilities [44].

To gain deeper insight into the structure of the newly synthesized MOFs, element-specific X-ray absorption spectroscopy was employed. The XANES (X-ray absorption near edge structure) part of the absorption spectrum is specifically sensitive to the oxidation state and coordination geometry, whereas the EXAFS region (extended X-ray absorption fine structure) provides information about local atomic structure, such as bond distances and coordination number. The Zr K-edge and Hf L_3-edge XAS data for Zr-MIL-140A and Hf-MIL-140A, respectively, were collected at the SuperXAS beamline of Swiss Light Source (Fig. 8).

The normalized Zr K-edge XANES spectrum of the Zr-MIL-140A is plotted in Fig. 8A along with the spectra collected for reference materials, metallic Zr foil (hexagonal close-packed structure) and ZrO_2 (monoclinic structure). As shown, significant differences were observed in the collected spectral profiles. The absorption edge position for Zr-

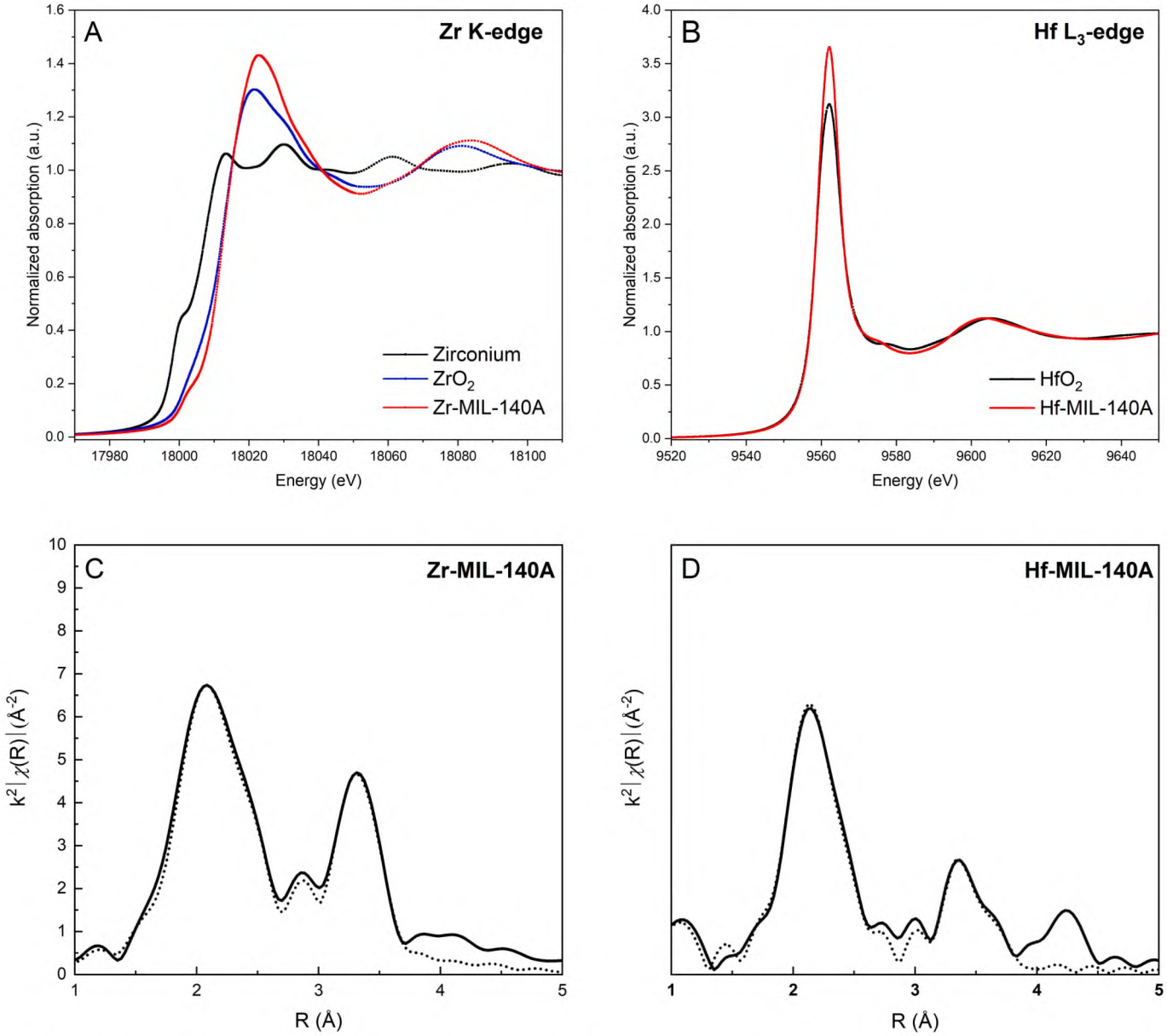

Fig. 8. X-ray absorption spectroscopy data for (Me – Zr or Hf)-MIL-140A samples. Normalized XANES spectra at **(A)** Zr K-edge of Zr-based materials and **(B)** Hf L_3-edge of Hf-based materials. Results of the EXAFS fitting: module of the Fourier transform (phase-corrected) of the EXAFS signal for **(C)** Zr-MIL-140A and **(D)** Hf-MIL-140A; experimental data are shown as solid line, whereas fitted curves are presented as dotted line.

MIL-140A, determined from the maximum of the first derivative of the absorption curve, was found to be 18012.8 eV. The edge position is similar to the value obtained for zirconium oxide (18013.0 eV) and much higher than for the metallic zirconium (17988.2 eV). This is consistent with the formation of the Zr (+IV) oxidation state in the synthesized MOF [45,46]. Moreover, the observed increase in the white line intensity (maximum of absorption edge) is attributed to the different chemical environments in the first coordination shell around Zr. In order to gain insight into the electronic structure, the experimental features can be interpreted based on the density of states calculated with the FEFF9.6 code (see Figure S14 in the Supporting Information). The intense main peak (white line) at 18023.0 eV is assigned to the dipole-allowed 1s-5p transitions, which is consistent with the values reported for the Zr-based carboxylate MOFs, (*e.g.*, UiO-66) [47]. The weak pre-edge feature observed at 18003.0 eV corresponds to the dipole-forbidden 1s → 4d transitions. These transitions are possible due to the partial d-p orbital mixing resulting from distortions in the centrosymmetry of the molecule. Therefore, the resulting pre-edge feature is extremely sensitive to the ligand environment and the symmetry of the metal center [48,49]. In like manner, the Hf L_3-edge XANES analysis was used to characterize the Hf species in the synthesized MOF. The normalized XANES spectra collected at Hf L_3-edge for the Hf-MIL-140A sample and standard material (monoclinic HfO_2) are shown in Fig. 8B. In both studied samples, hafnium is present in the (+IV) oxidation state as determined by the maxima of the first derivative of the data (9559.3 eV for Hf-MIL-140A). Given that L_3-edge XANES directly probes the $2p_{3/2}$ → 5d electronic transitions, the intensity of the white line reflects the population of the unoccupied 5d states as well as the difference in the local environment of Hf species. The higher intensity of the white line for Hf-based microporous crystalline materials (MOFs, zeolites) as compared to the HfO_2 standard was already reported in the literature [50,51].

To gain more insight into the nature of the Zr and Hf species in the synthesized MOFs, the local structure around the atoms was studied by extended X-ray absorption spectroscopy. The Fourier transforms of the metal k^2-weighted spectra are shown in Fig. 8C and 8D (complementary information, such as k-space FT-EXAFS is shown in Figure S15). Fitting of the Fourier-transformed extended X-ray absorption fine structure (FT-EXAFS) data may provide insight into the structural parameters such as coordination number (CN), bond distance, and local disorder (Debye-Waller factor) (Table S8). The best fitting parameters, obtained using the Artemis program from the Demeter software package [52], are summarized in Table S8. As can be seen, the simulated spectra perfectly match the experimental one which indicates that our model and assumptions are realistic. In addition, our results are in agreement with those previously reported for Zr and Hf-based MOFs [47,51]. For the Zr-MIL-140A sample, three shell contributions could be identified in the R space (phase corrected, Fig. 8C), with two dominating peaks, ascribed to Zr-O scattering paths, at 2.08 Å and 2.21 Å with CN = 4.2 and 4.5, respectively. Those paths are related to the closest neighbors of the zirconium (IV) atom, corresponding to overlapping features of the Zr-$O_{\mu 3\text{-}O}$ (bridging oxygen) and Zr-O_{COO} (oxygen connected to the carboxylate groups from bridging terephthalates). The third feature is ascribed to the Zr-Zr scattering path at *ca.* 3.27 Å with CN of 1.6. For the Hf-MIL-140 sample, similar analysis was performed. In the EXAFS spectra four shell contributions could be identified in the R space (Fig. 8D), with two dominating peaks ascribed to Hf-O scattering paths at *ca.* 2.08 Å and 2.19 Å with CN = 5.0 and 2.4, respectively, the third scattering path ascribed to Hf-O at *ca.* 3.17 Å and CN = 1.6 and fourth ascribed to Hf-Hf at *ca.* 3.28 Å with CN equal to 0.8.

4. Conclusions

In this work, the preparation of pure (Me – Zr or Hf)-MIL-140A from a mixture of UiO-66/MIL-140A by using the sonochemical approach is developed. For the first time, the synthesis of the Hf-MIL-140A structure is presented.

Based on SR-PXRD and cRED analysis, it was determined that the Hf-MIL-140A structure is isostructural to the Zr-MIL-140A structure. The results of low-temperature N_2 sorption analysis have shown that the sonochemical treatment of UiO-66/MIL-140A mixture results in the increase of the specific BET surface area up to 653 m^2/g which is 1.5 higher than reported for conventional synthesis [10]. The Hf-MIL-140A exhibited S_{BET} equal to 425 m^2/g which is twice as high as for Ce-MIL-140A obtained using microwave synthesis [17]. The increase of both specific surface and pore volume in MIL-140A samples prepared using the developed sonochemical route is due to the formation of structural defects during the synthesis step. The presence of structural defects was confirmed by low-temperature N_2 adsorption and by the STEM analysis of prepared samples, which revealed that the surfaces of both Zr- and Hf-MIL-140A samples are evenly covered with slit-like structural defects. XANES and EXAFS analysis provided additional insight into the nature of the Zr and Hf species in the newly synthesized MOFs. The data revealed the presence of metal-bridging oxygen and oxygen connected to the carboxylate groups from bridging terephthalates.

5. Outlook

The sonochemical irradiation method developed in this study allowed to obtain the pure MIL-140A MOFs from a mixture of UiO-66/MIL-140A. The proposed method results in a considerable increase of both BET surface area and pore volume through generated slit-like structure defects during post-synthetic treatment.

The synthesis of a Hf-MIL-140A structure by using a sonochemical route opens new strategies in MOF synthesis and development at the laboratory scale. Since the sonochemical route presented in this manuscript was devoted to the fundamental research on synthesis of metal–organic frameworks, prospective detailed scale-up studies are highly demanded. The synergic effect of ultrasound irradiation and the presence of concentrated acetic acid results in the formation of defective structure which on one side results in a more open structure through slit-like cavities and the increase of Lewis acidity due to the missing nodes on the other [44]. The latter is highly anticipated to develop novel porous materials for the application of gas storage, radioactive waste removal, catalysis, and drug delivery, where the presence of high specific surface areas, pore volumes, and structure defects are highly demanded. Therefore, it is anticipated that the Hf-based stable and durable MOFs will be in the spotlight of scientists in the field of metal–organic framework engineering.

Additionally, sonochemical irradiation has proven its unique properties in the post-synthesis MOFs treatment, which was not previously described in the literature. Although sonochemical irradiation was successfully used to synthesize various MOF structures, the information on its application in post-synthesis treatment is scarce. Therefore, the further development of mechanisms and the influence of sonochemical parameters on crystal structure parameters and on a synthesis of pure MOF phase from a mixture of various MOFs should be further investigated.

CCDC 2236688–2236689 contains the supplementary crystallographic data for this paper. These data can be obtained free of charge from The Cambridge Crystallographic Data Centre via https://www.ccdc.cam.ac.uk/structures.

CRediT authorship contribution statement

Przemysław J. Jodłowski: Conceptualization, Methodology, Validation, Investigation, Resources, Data curation, Writing – review & editing, Visualization, Supervision, Funding acquisition. **Grzegorz Kurowski:** Investigation, Validation. **Klaudia Dymek:** Investigation, Validation. **Marcin Oszajca:** Methodology, Validation, Investigation, Writing – review & editing. **Witold Piskorz:** Methodology, Validation, Investigation, Writing – review & editing. **Kornelia Hyjek:**

Investigation, Validation. **Anna Wach:** Methodology, Validation, Investigation, Writing – review & editing. **Anna Pajdak:** Methodology, Validation, Investigation, Writing – review & editing. **Michal Mazur:** Methodology, Validation, Investigation, Writing – review & editing. **Daniel N. Rainer:** Methodology, Validation, Investigation, Writing – review & editing. **Dominik Wierzbicki:** Methodology, Validation, Investigation, Writing – review & editing. **Piotr Jeleń:** Investigation. **Maciej Sitarz:** Investigation.

Declaration of Competing Interest

The authors declare that they have no known competing financial interests or personal relationships that could have appeared to influence the work reported in this paper.

Acknowledgments

The work was supported by the National Science Centre, Poland, under research project "MOF-antidote: Novel detoxification materials based on metal-organic frameworks for drugs of abuse removal – synthesis, chemical characterization, toxicity and efficacy in in vivo and in vitro studies", no. UMO-2021/43/B/NZ7/00827.

D.N.R. and M.M. acknowledge the OP VVV "Excellent Research Teams", project No. CZ.02.1.01/0.0/0.0/15_003/0000417 – CUCAM for financial support.

The Paul Scherrer Institute, Villigen, Switzerland, is acknowledged for provision of synchrotron radiation for *ex-situ* measurements at beamline SuperXAS (X10DA) and MS Beamline X04SA of the SLS.

Appendix A. Supplementary data

Supplementary data to this article can be found online at https://doi.org/10.1016/j.ultsonch.2023.106377.

References

[1] M. Taddei, When defects turn into virtues: The curious case of zirconium-based metal-organic frameworks, Coord. Chem. Rev. 343 (2017) 1–24, https://doi.org/10.1016/j.ccr.2017.04.010.

[2] S. Leubner, V.E.G. Bengtsson, K. Synnatschke, J. Gosch, A. Koch, H. Reinsch, H. Xu, C. Backes, X. Zou, N. Stock, Synthesis and Exfoliation of a New Layered Mesoporous Zr-MOF Comprising Hexa- A nd Dodecanuclear Clusters as Well as a Small Organic Linker Molecule, J. Am. Chem. Soc. 142 (37) (2020) 15995–16000.

[3] O.M. Yaghi, H. Li, Hydrothermal Synthesis of a Metal-Organic Framework Containing Large Rectangular Channels, J. Am. Chem. Soc. 117 (1995) 10401–10402, https://doi.org/10.1021/ja00146a033.

[4] J.H. Cavka, S. Jakobsen, U. Olsbye, N. Guillou, C. Lamberti, S. Bordiga, K. P. Lillerud, A new zirconium inorganic building brick forming metal organic frameworks with exceptional stability, J. Am. Chem. Soc. 130 (42) (2008) 13850–13851.

[5] J.E. Mondloch, W. Bury, D. Fairen-Jimenez, S. Kwon, E.J. DeMarco, M.H. Weston, A.A. Sarjeant, S.T. Nguyen, P.C. Stair, R.Q. Snurr, O.K. Farha, J.T. Hupp, Vapor-phase metalation by atomic layer deposition in a metal-organic framework, J. Am. Chem. Soc. 135 (28) (2013) 10294–10297.

[6] V. Bon, I. Senkovska, I.A. Baburin, S. Kaskel, Zr- and Hf-based metal-organic frameworks: Tracking down the polymorphism, Cryst. Growth Des. 13 (2013) 1231–1237, https://doi.org/10.1021/cg301691d.

[7] D. Feng, W.-C. Chung, Z. Wei, Z.-Y. Gu, H.-L. Jiang, Y.-P. Chen, D.J. Darensbourg, H.-C. Zhou, Construction of Ultrastable Porphyrin Zr Metal – Organic Frameworks through Linker Elimination, J. Am. Chem. Soc. 135 (45) (2013) 17105–17110.

[8] J. Winarta, B. Shan, S.M. Mcintyre, L. Ye, C. Wang, J. Liu, B. Mu, A Decade of UiO-66 Research: A Historic Review of Dynamic Structure, Synthesis Mechanisms, and Characterization Techniques of an Archetypal Metal-Organic Framework, Cryst. Growth Des. 20 (2) (2020) 1347–1362.

[9] T.A. Makal, A.A. Yakovenko, H.C. Zhou, Isomerism in metal-organic frameworks: "Framework isomers", J. Phys. Chem. Lett. 2 (2011) 1682–1689, https://doi.org/10.1021/jz200424h.

[10] V. Guillerm, F. Ragon, M. Dan-Hardi, T. Devic, M. Vishnuvarthan, B. Campo, A. Vimont, G. Clet, Q. Yang, G. Maurin, G. Férey, A. Vittadini, S. Gross, C. Serre, A series of isoreticular, highly stable, porous zirconium oxide based metal-organic frameworks, Angew. Chemie – Int. Ed. 51 (37) (2012) 9267–9271.

[11] J. Pires, J. Fernandes, K. Dedecker, J.R.B. Gomes, G. Pérez-Sánchez, F. Nouar, C. Serre, M.L. Pinto, Enhancement of Ethane Selectivity in Ethane-Ethylene Mixtures by Perfluoro Groups in Zr-Based Metal-Organic Frameworks, ACS Appl. Mater. Interfaces 11 (30) (2019) 27410–27421.

[12] W. Liang, R. Babarao, T.L. Church, D.M. D'Alessandro, Tuning the cavities of zirconium-based MIL-140 frameworks to modulate CO2 adsorption, Chem. Commun. 51 (2015) 11286–11289, https://doi.org/10.1039/c5cc02539g.

[13] M. Schulz, N. Marquardt, M. Schäfer, T. Heinemeyer, A. Schaate, Solvent-assisted linker exchange as a tool for the design of mixed-linker MIL-140D structured MOFs for highly selective detection of gaseous H2S, RSC Adv. 10 (2020) 12334–12338, https://doi.org/10.1039/d0ra01164a.

[14] N.Z.S. Yahaya, S.H. Paiman, N. Abdullah, N. Mu'ammar Mahpoz, A.A. Raffi, M. A. Rahman, K.H. Abas, A.A. Aziz, M.H.D. Othman, J. Jaafar, Synthesis and characterizations of MIL-140B-Al2O3/YSZ ceramic membrane using solvothermal method for seawater desalination, J. Aust. Ceram. Soc. 56 (1) (2020) 291–300.

[15] J. Yang, J.J. Ma, D.M. Zhang, T. Xue, Y.J. Guan, Effect of organic moieties (phenyl, naphthalene, and biphenyl) in Zr-MIL-140 on the hydrogenation activity of Pd nanoparticles, Chinese Chem. Lett. 27 (2016) 1679–1682, https://doi.org/10.1016/j.cclet.2016.04.015.

[16] M. Lammert, M.T. Wharmby, S. Smolders, B. Bueken, A. Lieb, K.A. Lomachenko, D. D. Vos, N. Stock, Cerium-based metal organic frameworks with UiO-66 architecture: Synthesis, properties and redox catalytic activity, Chem. Commun. 51 (63) (2015) 12578–12581.

[17] J. Jacobsen, L. Wegner, H. Reinsch, N. Stock, Ce-MIL-140: expanding the synthesis routes for cerium(iv) metal-organic frameworks, Dalt. Trans. 49 (2020) 11396–11402, https://doi.org/10.1039/d0dt02455d.

[18] M. Schulz, N. Marquardt, M. Schäfer, D.P. Warwas, S. Zailskas, A. Schaate, A Low-Temperature Approach for the Phase-Pure Synthesis of MIL-140 Structured Metal-Organic Frameworks, Chem. – A Eur. J. 25 (2019) 13598–13608, https://doi.org/10.1002/chem.201902981.

[19] H. Xu, B.W. Zeiger, K.S. Suslick, Sonochemical synthesis of nanomaterials, Chem. Soc. Rev. 42 (2013) 2555–2567, https://doi.org/10.1039/C2CS35282F.

[20] K.S. Suslick, Sonochemistry, Science 247 (1990) 1439–1445, https://doi.org/10.1126/science.247.4949.1439.

[21] H. Kim, K. Suslick, The Effects of Ultrasound on Crystals: Sonocrystallization and Sonofragmentation, Crystals 8 (2018) 280, https://doi.org/10.3390/cryst8070280.

[22] L.-G. Qiu, Z.-Q. Li, Y. Wu, W. Wang, T. Xu, X. Jiang, Facile synthesis of nanocrystals of a microporous metal–organic framework by an ultrasonic method and selective sensing of organoamines, Chem. Commun. (2008) 3642, https://doi.org/10.1039/b804126a.

[23] W.-J. Son, J. Kim, J. Kim, W.-S. Ahn, Sonochemical synthesis of MOF-5, Chem. Commun. (2008) 6336, https://doi.org/10.1039/b814740j.

[24] T. Chalati, P. Horcajada, R. Gref, P. Couvreur, C. Serre, Optimisation of the synthesis of MOF nanoparticles made of flexible porous iron fumarate MIL-88A, J. Mater. Chem. 21 (2011) 2220–2227, https://doi.org/10.1039/c0jm03563g.

[25] R. Sabouni, H. Kazemian, S. Rohani, A novel combined manufacturing technique for rapid production of IRMOF-1 using ultrasound and microwave energies, Chem. Eng. J. 165 (2010) 966–973, https://doi.org/10.1016/j.cej.2010.09.036.

[26] S. Jakobsen, D. Gianolio, D.S. Wragg, M.H. Nilsen, H. Emerich, S. Bordiga, C. Lamberti, U. Olsbye, M. Tilset, K.P. Lillerud, Structural determination of a highly stable metal-organic framework with possible application to interim radioactive waste scavenging: Hf-UiO-66, Phys. Rev. B - Condens. Matter Mater. Phys. 86 (12) (2012), https://doi.org/10.1103/PhysRevB.86.125429.

[27] B. Miljevic, F. Hedayat, S. Stevanovic, K.E. Fairfull-Smith, S.E. Bottle, Z. D. Ristovski, To sonicate or not to sonicate PM filters: Reactive oxygen species generation upon ultrasonic irradiation, Aerosol Sci. Tech. 48 (2014) 1276–1284, https://doi.org/10.1080/02786826.2014.981330.

[28] J. Chu, F.-S. Ke, Y. Wang, X. Feng, W. Chen, X. Ai, H. Yang, Y. Cao, Facile and reversible digestion and regeneration of zirconium-based metal-organic frameworks, Commun. Chem. 3 (1) (2020), https://doi.org/10.1038/s42004-019-0248-7.

[29] Y. Feng, Q. Chen, M. Jiang, J. Yao, Tailoring the Properties of UiO-66 through Defect Engineering: A Review, Ind. Eng. Chem. Res. 58 (2019) 17646–17659, https://doi.org/10.1021/acs.iecr.9b03188.

[30] C.A. Clark, K.N. Heck, C.D. Powell, M.S. Wong, Highly Defective UiO-66 Materials for the Adsorptive Removal of Perfluorooctanesulfonate, ACS Sustain. Chem. Eng. 7 (2019) 6619–6628, https://doi.org/10.1021/acssuschemeng.8b05572.

[31] B. Bueken, N. Van Velthoven, A. Krajnc, S. Smolders, F. Taulelle, C. Mellot-Draznieks, G. Mali, T.D. Bennett, D. De Vos, Tackling the Defect Conundrum in UiO-66: A Mixed-Linker Approach to Engineering Missing Linker Defects, Chem. Mater. 29 (24) (2017) 10478–10486.

[32] J.K. Bristow, K.L. Svane, D. Tiana, J.M. Skelton, J.D. Gale, A. Walsh, Free energy of ligand removal in the metal-organic framework UiO-66, J. Phys. Chem. C 120 (2016) 9276–9281, https://doi.org/10.1021/acs.jpcc.6b01659.

[33] M. Vandichel, J. Hajek, F. Vermoortele, M. Waroquier, D.E. De Vos, V. Van Speybroeck, Active site engineering in UiO-66 type metal-organic frameworks by intentional creation of defects: A theoretical rationalization, CrstEngComm 17 (2015) 395–406, https://doi.org/10.1039/c4ce01672f.

[34] G.C. Shearer, S. Chavan, S. Bordiga, S. Svelle, U. Olsbye, K.P. Lillerud, Defect Engineering: Tuning the Porosity and Composition of the Metal-Organic Framework UiO-66 via Modulated Synthesis, Chem. Mater. 28 (2016) 3749–3761, https://doi.org/10.1021/acs.chemmater.6b00602.

[35] T. Yang, T. Willhammar, H. Xu, X. Zou, Z. Huang, Single-crystal structure determination of nanosized metal–organic frameworks by three-dimensional electron diffraction, Nat. Protoc. 17 (2022) 2389–2413, https://doi.org/10.1038/s41596-022-00720-8.

[36] S. Smeets, B. Wang, E. Hogenbirk, instamatic-dev/instamatic: 1.7.0, (2021). doi: 10.5281/ZENODO.5175957.

[37] J.P. Glusker, Biological crystallography, Acta Crystallogr. Sect. D 49 (1993) 1, https://doi.org/10.1107/S090744499201028X.
[38] G.M. Sheldrick, SHELXT - Integrated space-group and crystal-structure determination, Acta Crystallogr. A 71 (2015) 3–8, https://doi.org/10.1107/S2053273314026370.
[39] G.M. Sheldrick, Crystal structure refinement with SHELXL, Acta Crystallogr. Sect. C Struct. Chem. 71 (2015) 3–8, https://doi.org/10.1107/S2053229614024218.
[40] S. Leubner, R. Siegel, J. Franke, M.T. Wharmby, C. Krebs, H. Reinsch, J. Senker, N. Stock, Design and Precursor-based Solid-State Synthesis of Mixed-Linker Zr-MIL-140A, Inorg. Chem. 59 (20) (2020) 15250–15261.
[41] G. Socrates, Infrared and Raman Characteristic Group Frequencies: Tables and Charts, Wiley, 2004.
[42] C. Atzori, G.C. Shearer, L. Maschio, B. Civalleri, F. Bonino, C. Lamberti, S. Svelle, K. P. Lillerud, S. Bordiga, Effect of Benzoic Acid as a Modulator in the Structure of UiO-66: An Experimental and Computational Study, J. Phys. Chem. C 121 (17) (2017) 9312–9324.
[43] G.C. Shearer, S. Chavan, J. Ethiraj, J.G. Vitillo, S. Svelle, U. Olsbye, C. Lamberti, S. Bordiga, K.P. Lillerud, Tuned to perfection: Ironing out the defects in metal-organic framework UiO-66, Chem. Mater. 26 (14) (2014) 4068–4071.
[44] Z. Hu, Y. Wang, D. Zhao, The chemistry and applications of hafnium and cerium (iv) metal-organic frameworks, Chem. Soc. Rev. 50 (2021) 4629–4683, https://doi.org/10.1039/d0cs00920b.
[45] V.V. Butova, K.S. Vetlitsyna-Novikova, I.A. Pankin, K.M. Charykov, A.L. Trigub, A. V. Soldatov, Microwave synthesis and phase transition in UiO-66/MIL-140A system, Microporous Mesoporous Mater. 296 (2020), 109998, https://doi.org/10.1016/j.micromeso.2020.109998.
[46] K.A. Lomachenko, J. Jacobsen, A.L. Bugaev, C. Atzori, F. Bonino, S. Bordiga, N. Stock, C. Lamberti, Exact Stoichiometry of Ce x Zr 6–x Cornerstones in Mixed-Metal UiO-66 Metal-Organic Frameworks Revealed by Extended X-ray Absorption Fine Structure Spectroscopy, J. Am. Chem. Soc. 140 (50) (2018) 17379–17383.
[47] Z. Su, Y.R. Miao, G. Zhang, J.T. Miller, K.S. Suslick, Bond breakage under pressure in a metal organic framework, Chem. Sci. 8 (2017) 8004–8011, https://doi.org/10.1039/c7sc03786d.
[48] K. Getty, M.U. Delgado-Jaime, P. Kennepohl, Assignment of pre-edge features in the Ru K-edge X-ray absorption spectra of organometallic ruthenium complexes, Inorganica Chim. Acta. 361 (2008) 1059–1065, https://doi.org/10.1016/j.ica.2007.07.029.
[49] R.V. Vedrinskii, E.S. Nazarenko, M.P. Lemeshko, V. Nassif, O. Proux, A. A. Novakovich, et al., Temperature dependent XAFS studies of local atomic structure of the perovskite-type zirconates, Phys. Rev. B – Condens. Matter Mater. Phys. 73 (2006) 1–8, https://doi.org/10.1103/PhysRevB.73.134109.
[50] L. Botti, S.A. Kondrat, R. Navar, D. Padovan, J.S. Martinez-Espin, S. Meier, C. Hammond, Solvent-Activated Hafnium-Containing Zeolites Enable Selective and Continuous Glucose-Fructose Isomerisation, Angew. Chemie – Int. Ed. 59 (45) (2020) 20017–20023.
[51] S. Rojas-Buzo, B. Bohigues, C.W. Lopes, D.M. Meira, M. Boronat, M. Moliner, A. Corma, Tailoring Lewis/Brønsted acid properties of MOF nodesviahydrothermal and solvothermal synthesis: simple approach with exceptional catalytic implications, Chem. Sci. 12 (29) (2021) 10106–10115.
[52] B. Ravel, M. Newville, ATHENA, ARTEMIS, HEPHAESTUS: Data analysis for X-ray absorption spectroscopy using IFEFFIT, J. Synchrotron Radiat. 12 (2005) 537–541, https://doi.org/10.1107/S0909049505012719.